

# Soil-pile interaction during pile installation. Observations from x-ray tomography and 3D-DIC

Matias SILVA<sup>a,b,1</sup> and Gaël COMBE<sup>a,b</sup>

<sup>a</sup> *Université Grenoble Alpes, 3SR, F-38000, Grenoble, France*

<sup>b</sup> *CNRS, 3SR, F-38000, Grenoble, France*

**Abstract.** The mechanisms behind the installation of a driven pile in sands are complex and difficult to identify from field tests. Phenomenon such as grain breakage, local variations in sand density, pile abrasion and arching effects, are commonly studied through indirect methods or by using small laboratory models. This article presents the results of an experimental laboratory research devoted to the analysis of the soil kinematics during the installation of an uninstrumented close-ended model pile in a specimen of siliceous sand. The research has focused on understanding the micromechanical aspects of the installation process by focusing on sand-pile interaction around the pile's tip. A three dimensional displacement field was obtained with the combined use of x-ray tomography and three dimensional digital image correlations. The results show two well-identified zones where the displacement and therefore strains concentrate. The interaction of these zones, which are linked by consecutive phases of sand contraction and extension as the pile embeds into the sand, gives new ideas about the mechanisms controlling the pile shaft friction.

**Keywords.** X-ray tomography; digital image correlation, pile installation, kinematics.

## 1. Introduction

The mechanisms behind the installation of driven piles in sands are complex and difficult to identify from field tests. Phenomenon such as grain breakage, local variations in sand density, pile abrasion and sand arching effects, are commonly studied through indirect methods or by using small laboratory models [1], [2], [3], [4].

Robinsky & Morrison [1] were among the first to address the problem of the response of the surrounding soil during the installation of a small model pile. Using x-ray radiographies, following lead shot deployed in the sand mass, Robinsky & Morrison observed the formation of a zone of loose sand around the pile during its installation. When a pile is pushed into a sand mass, the sand near the pile's surface is dragged down with the pile movement under the constant confinement of the surrounding soil, resulting in the formation of an arc of sand around the pile. These conclusions were later confirmed by other authors from density measurements on large calibration chamber tests [5], photoelastic observations on a plain strain model [3] and

---

<sup>1</sup> Corresponding Author. Laboratoire 3SR, Domaine Universitaire, BP53, 38041 Grenoble Cedex 9, France E-mail: matias.silva@3sr-grenoble.fr

from x-ray absorption analyses [6], [7], [8]. In addition, results from Particle Image Velocimetry (PIV) on a plain strain model [4] suggested that a zone of high density will develop around the pile as the latter embeds deeper into the sand mass. These results show irrecoverable volume reduction beneath the pile tip as a result of particle breakage and soil compaction due to the high stresses developed at the advancing pile tip [3]. As the pile installation progresses into this highly overconsolidated sand [4], a zone of high density will be created around the pile shaft. The cylindrical cavity collapse of this highly compacted sand layer may lead to reductions in radial stress and to the development of an arching effect similar to that observed earlier by Robinsky & Morrison [1]. Plain strain analyses [4] also showed a series of strain path reversals with the sand mass around the pile tip experiencing consecutive stages of local compressive and dilatant phases.

This paper presents the first results of an experimental programme devoted to the analysis of the kinematics developed in the soil mass during the installation of a model pile into a siliceous sand specimen using micro tomography (X-ray micro CT) and three dimensional (3D) digital image correlation (DIC).

## 2. Experimental arrangements

### 2.1. General Arrangements

The tests were conducted in the micro computed (CT) tomograph of the laboratory 3SR in Grenoble, France. A pseudo-triaxial cell capable of applying several lateral confining pressures to a sand specimen during a tomography scan was designed and built, inside which an uninstrumented 5 mm diameter cone-ended smooth aluminium (pile roughness of  $\pm 0.7 \mu\text{m}$ ) model pile was installed by monotonic loading.

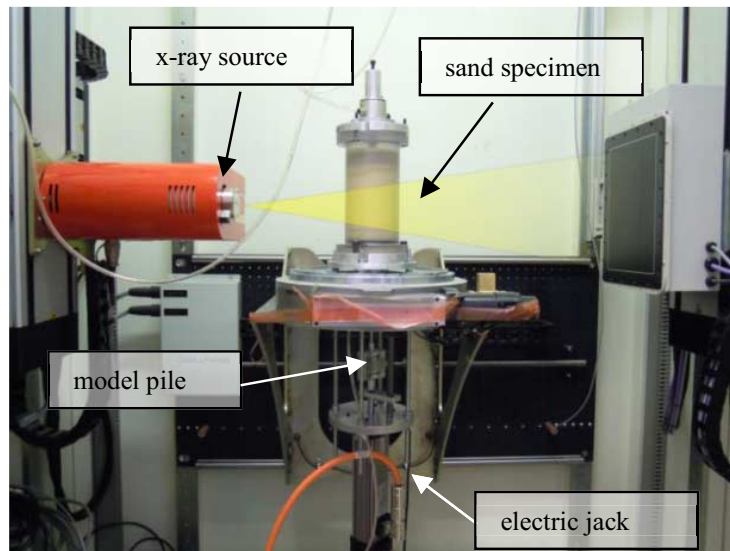


**Figure 1:** Test arrangements during x-ray micro tomography.

The sample consists of a cylinder 70 mm in diameter and 100 mm in height of dry Fontainebleau NE34 siliceous sand (see Table 1). Samples were prepared by four consecutive layers 25 mm high and a density of  $1.60 \text{ kg/m}^3$ , corresponding to a relative density,  $D_r$ , of approximately 70%. A constant isotropic confining pressure of 100 kPa was applied to the specimen during pile installation and X-ray scanning

through a water-air interface similar to a triaxial test. The pile installation took place within an hour after pressurization. Important scale and boundary effects are expected to occur due to the reduced size of the model pile with respect to the confining boundary and with respect to the mean particle size,  $d_{50}$ . If we consider our experiment as a small pressurised laboratory calibration chamber, a ratio of pile diameter,  $D$ , to the chamber diameter,  $B$ , of at least 60 should be considered to avoid boundary effects, as reported by several authors from experimental [10], [11] and numerical analyses, [12]. In addition, a size effect is also expected from the small ratio of the pile diameter,  $D$ , to mean particle size,  $d_{50}$ , [13].

**Table 1:** Index properties of Fontainebleau NE34 sand

$e_{\min}$	$e_{\max}$	$d_{10}$ (mm)	$d_{50}$ (mm)	$d_{60}$ (mm)
0.51	0.90	0.15	0.21	0.23

## 2.2. X-ray micro CT

Due to the predefined sand sample and pile diameter, scans were set to a tension of 200 kV and a current of 150  $\mu$ A. This configuration allows for a spatial resolution of approximately 23, and 43  $\mu$ m/pixel for global and local tomographies respectively (scans of the entire sample volume, or scans focusing on the pile tip). There were 1024 radiographies made of the sand sample for the reconstruction of the entire volume. Using micro CT, a 3D digital image of the x-ray attenuation in the soil sample and the pile was obtained. An example of the reconstructed volume during a local tomography is presented in Figure 2.

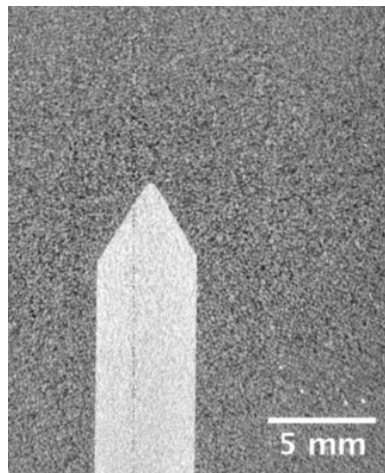


Figure 2: Vertical slice across the sand sample during local tomography.

Due to the configuration of the 3SR tomograph's cabin, the pile was installed into the sand mass from the bottom section of the sample (in an upward movement). The pile embedded length was limited to 50 mm in order for the pile tip to be positioned approximately at the middle of the sample. This preparation aimed at avoiding boundary problems with the bottom part of the sample, with an allowance for subsequent pile displacement for Digital Image Correlation analysis.

The pile was installed using an electric jack into the sand mass at a rate of 0.1 mm/s, where a first tomogram was taken. The pile head load was kept constant during the different tests. Several tomograms were then obtained after incremental pile displacements, ranging from 0.5 to 3.0 mm, to perform further digital image correlation

analysis in order to evaluate the incremental displacement field between consecutive loading steps.

### 2.3. 3D-Digital Image Correlation

In order to perform an image correlation between two images, it is first required to define a regular grid of analysis points (*Node Spacing, NS*) over the reference image; then, a group of pixels or correlation window (*CW*) is defined for each node of the grid. Image correlation is performed, for each node, by identifying the most similar *CW* in the deformed image based on statistical measures of correlation of the images within each subset, and mapping functions between the subsets. Different measures can be used to assess the degree of similarity of the subset images. In this particular case, correlation between images is estimated based on equation 1:

$$\frac{\sum_{x,y} [I1(x,y) \cdot I2(x+u,y+v)]}{\sqrt{\sum_{x,y} [I1(x,y)^2 \cdot I2(x+u,y+v)^2]}} \quad (1)$$

where  $x$  and  $y$  are the (2D) spatial coordinates,  $u$  and  $v$  the displacements of a pixel from image 1 ( $I1$ ) to a new position in image 2 ( $I2$ ). In the case of rigid body displacements of a subset,  $u$  and  $v$ , will be constant for all  $(x, y)$  positions in that *CW*. An analogy of equation 1 is used for the estimation of the correlation coefficient in three dimensions. Sub-pixel refinement techniques are required, by interpolating the correlation coefficient between two images by a polynomial or surface function, to estimate the maximum value which will correspond to a non integer value (lower than one pixel). DIC analysis is completed with strain calculations, which are based on the gradients of the derived displacements and a continuum assumption.

The results presented in the following sections were derived using the 3D-DIC code TomoWarp [14], [15]. The full strain tensor field in the form of volumetric strain and maximum shear (distortional) strains was derived. This code calculates the strains from the derived displacements under continuum assumptions. The experimental programme and the parameters considered for DIC calculations are outlined in Table 2.

**Table 2:** Summary of experimental programme

Test ID	Pile head displacement (mm)	NS (pixels)	CW(pixels $\times$ pixels)	Resolution ( $\mu\text{m}$ )
T1	0.5	10	30	23.57
T2	1.0	10	30	23.57
T3	2.0	10	30	23.57
T4	2.0	7	15	43.55
T5	3.0	7	15	43.55

## 3. Results

Displacement contours following pile installation are plotted in the vertical and radial axes with respect to pile position at normalised distances from the pile axis,  $r/R$ , and by the normalised distance to the pile tip,  $h/R$ ,  $r$  and  $h$  being the distance to the pile's axis and to the pile radius,  $R$ , respectively.

Since DIC results are fully three-dimensional, the results presented in the following section represent the mean value of those displacement/strain points at a specific spatial distance to the pile/tip axis. As a sign convention, displacements are

considered to be positive when moving away from the pile axis. Positive strains represent extension.

### 3.1. Soil displacement

Vertical and horizontal displacements were combined to represent the radial displacements due to the (almost) axisymmetric condition of the experiments. Pile alignment was considered for the  $h/R$  and  $r/R$  normalised distances. Figures 3 a) and b) presents contour plots of the soil radial and vertical displacements respectively during test T2. The horizontal displacements reach maxima approximately when the pile tip passes the soil horizon. On the contrary, maximum vertical displacements are attained before the tip has reached the soil horizon, in this case at a distance of one pile diameter above the soil level.

In both figures, displacements concentrate in two well-identified zones around the pile tip. The first one is located beneath the tip and extends downwards 4 times the pile radius. The sand mass follows the pile movements, spreading away radially as the pile advances. Within this zone, a bulb in the vicinity of the tip concentrates most of the vertical displacements. A second zone, in some cases almost completely isolated from the surrounding sand mass, is observed behind the base of the cone tip at a distance of 1 to 1.5  $h/R$ .

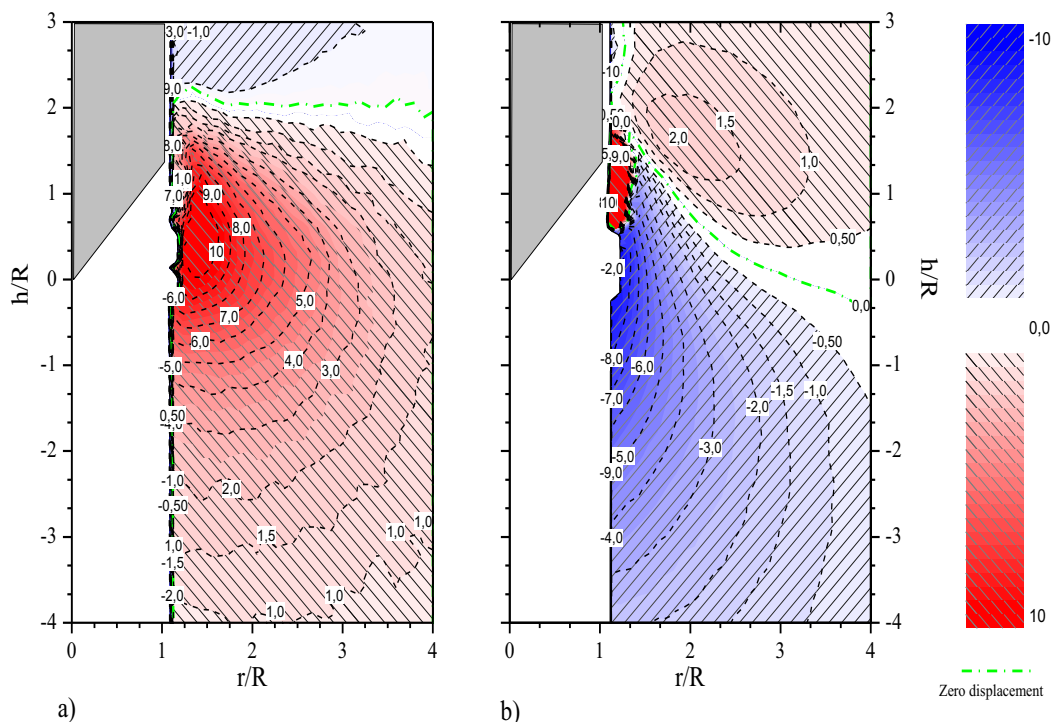


**Figure 3:** Incremental displacement after a 2 mm pile head displacement (values in pixels, 1 pixel = 45  $\mu\text{m}$ ): a) radial and b) vertical displacement considering a node spacing of 10 pixels during T3 test.

The soil in this region experiences an upward displacement opposite to the pile movement. The extension and maximum values are significantly lower compared to those observed beneath the tip and this zone is not in direct contact with the pile surface. The extension of these zones is directly linked to the imposed pile head displacement, in this case of 1 mm (Table 2). During tests T4 and 5, radial and vertical displacements are observed at distances greater than 6 times the pile radius.

In addition to the identification of displacement contour, it is also possible to observe an area in both Figures 3a) and b) where no displacements are observed. These ‘limit’ lines (segmented green lines in Figures 3a) and b)) mark out the boundary limits. We note that radial displacements are observed in a wider area radially from the central pile axis, but to a limited depth. On the contrary, vertical displacements are visible to a greater depth, but to a lesser extent from the pile axis. Figure 4 presents a summary for tests T1-T3 of the spatial position of these boundary lines.

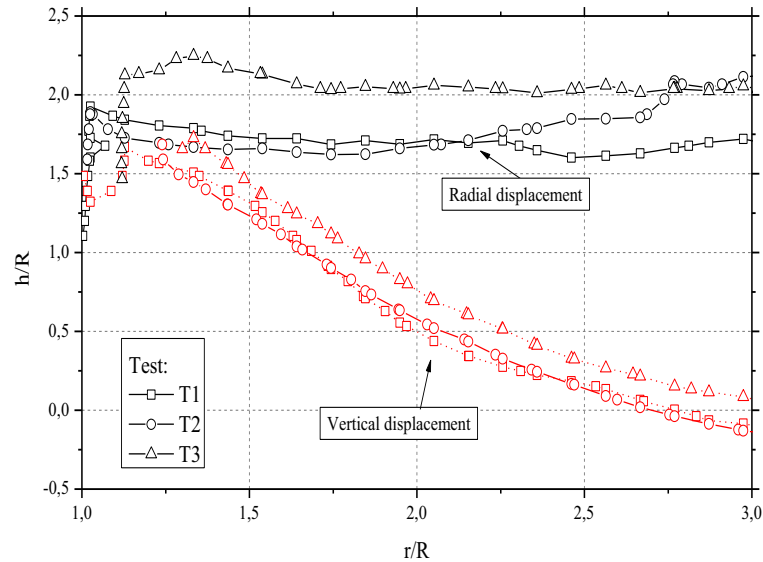


**Figure 4:** Position of zero radial and vertical displacement contours with respect to  $h/R$  and  $r/R$  after Figures 3a) and b)

### 3.2. Strain field

The analysis of strain patterns coming from the measurements of gradients on the kinematic field during a loading step can be characterised by Figures 5a) and b). A zone of high vertical contraction and radial extension develops beneath the pile tip as the pile is continuously pushed into the sand. A zone of high compaction will develop in front of the advancing tip. Some of the points were removed from the graphs, due to the large variations observed. Between two consecutive images, the characteristic pattern required to perform DIC is highly modified due to the irrecoverable changes in the sand microstructure.

Above this zone and oriented almost perpendicularly to the cone tip edge, the vertical extension and radial compression develop. These results agree with those obtained using plain strain models [4].

Figure 6 presents the volumetric strain after a 2 mm pile head displacement during test T4. The interaction between the different phases of vertical and horizontal contraction and extension presented in Figure 5, suggests that the soil beneath the tip undergoes an increase in volumetric strain leading to a lower relative density. It is not yet completely clear whether similar observations also apply for the sand mass in the vicinity of the cone edge where high degree of disturbance renders DIC analysis difficult. Results from Figure 6 are consistent with the analyses from X-ray absorption on similar specimens [16] which show a reduction in sand density around the pile.

Unlike what is observed in Figure 3 (and summarized in Figure 4 for the soil displacements), the boundary between the phases of radial/vertical contraction and

extension where no strain develops presents similar orientations with respect to the pile position. These results confirm what was observed using PIV techniques on a plain strain model [4].

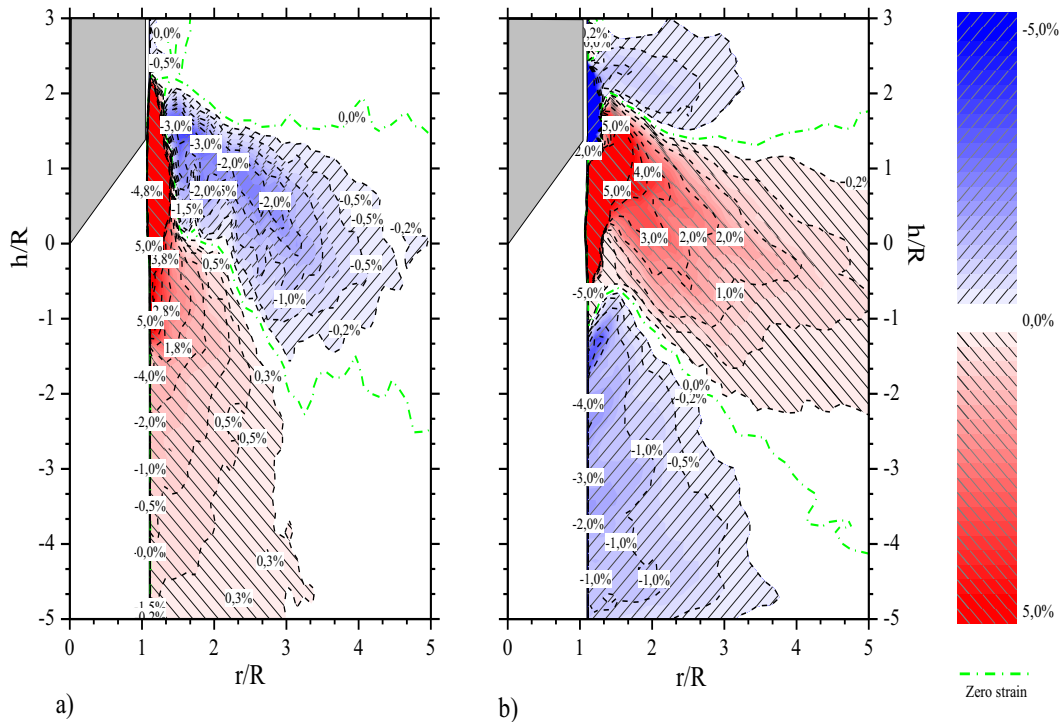


**Figure 5:** Radial (a) and vertical (b) strains after a 2 mm pile head displacement during test T4. Values in %.

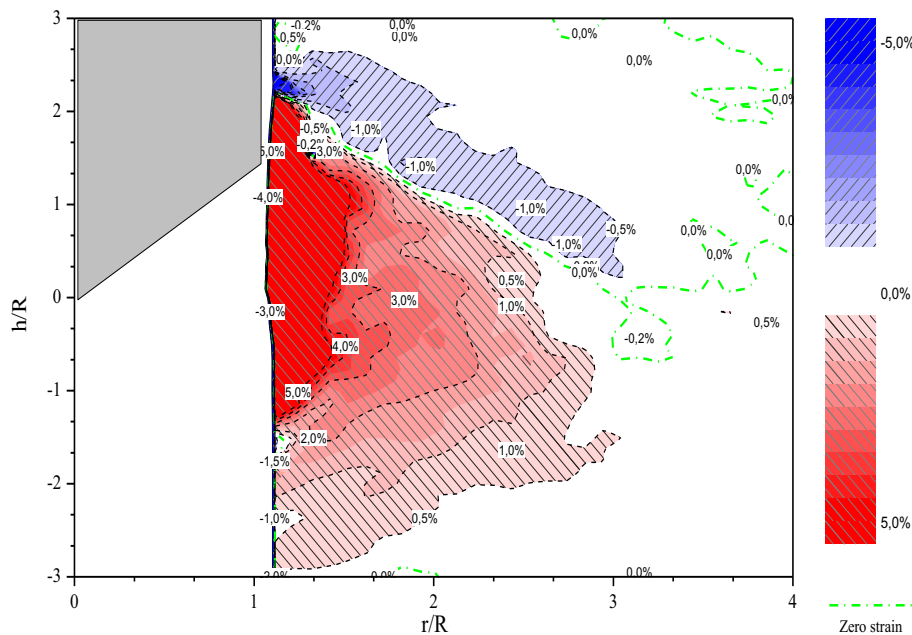


**Figure 6:** Volumetric strain after a 2 mm pile head displacement during test T4. Values in %.

Strains tend to develop mostly in the vicinity of the pile tip, in this case, to a maximum distance of five times the pile radius both vertically and radially. Taking into account an imposed pile head displacement of almost 20% pile diameter, it is possible that the flexible-constant pressure boundary condition influences the results, leading to mainly displacements in the soil without high degree of strains.



#### 4. Conclusions & Perspectives

The combined use of X-ray micro CT with 3D-DIC helps to understand the kinematics behind the installation of a model pile in a sand specimen. The results show two clearly distinct zones where vertical and radial displacements concentrate inside the sand mass. The sand particles on the shaft side of the cone tip seem to undergo vertical movements opposite to the direction in which the pile is driven.

The analysis of vertical and horizontal strain distribution shows clear trends of vertical compaction and radial extension for sand particles beneath the pile tip. On the contrary, the particles aligned perpendicularly to the tip edge behave in the opposite way, presenting radial compaction and vertical extension.

The results from DIC showed a reduction in density beneath the pile tip and around the pile shaft. The effect of particle breakage should be investigated within this zone. Further work should also analyse the effect of lateral pressure and boundary effects in the observed sand kinematics.

#### References

- [1] Robinsky, E. I., & Morrison, C. (1964). Sand displacement and compaction around model friction piles. *Canadian Geotechnical Journal*, **1**(2), 81–93.
- [2] Biarez, J., & Gresillon, J. (1972). Essais et suggestions pour le calcul de la force portante des pieux en milieu pulvérulent. *Geotechnique*, **22**(2), 433–450.
- [3] Allersma, H. G. B. (1988). Optical analysis of stress and strain around the tip of a penetrating probe. *Penetration Testing 1988*, Vol. 2, 615–620, Balkema, Rotterdam.
- [4] White, D. J., & Bolton, M. D. (2004). Displacement and strain paths during plane-strain model pile installation in sand. *Géotechnique*, **54**(6), 375–397.
- [5] Chong, M. K. (1988). Density changes of sand on cone penetration resistance. *Penetration Testing 1988*, Vol. 2, 707–714, Balkema, Rotterdam.
- [6] Van Nes, J. H. . (2004). Application of computerized tomography to investigate strain fields caused by cone penetration in sand. (Master's thesis). Delft University of Technology.
- [7] Ngan-Tillard, D., Cheng, X. H., Van Ness, J., & Zitha, P. L. J. (2005). Application of x-ray computed tomography to cone penetration tests in sands. *Proceedings of the Geo-Frontiers, Site Characterization and Modeling*, 1–12.
- [8] Morita, K., Otani, J., Mukunoki, T., Hironaka, J., & Pham, K. D. (2007). Evaluation of vertical and lateral bearing capacity mechanisms of pile foundations using X-ray CT. *Advances in Deep Foundations: International Workshop on Recent Advances of Deep Foundations*, 217–223.
- [9] Jardine, R., Zhu, B., Foray, P., & Yang, Z. (2013). Interpretation of stress measurements made around closed-ended displacement piles in sand. *Geotechnique*, **63**(8), 613–627.
- [10] Lunne, T., P. Robertson, and J. Powell (1997). *Cone Penetration Testing in Geotechnical Practice*. Blackie Academic, EF Spon/Routledge Publishers, New York.
- [11] Bolton, M. D., Gui, M. W., Garnier, J., Corte, J. F., Bagge, G., Laue, J., & Renzi, R. (1999). Centrifuge cone penetration tests in sand. *Géotechnique*, **49**(4), 543–552.
- [12] Salgado, R., J. Mitchell, and M. Jamiolkowski (1998). Calibration chamber size effects on penetration resistance in sand. *Journal of Geotechnical and Geoenvironmental Engineering*, **124** (9), 878-888.
- [13] Garnier, J. (2002). Size effects in shear interfaces. In *Constitutive and Centrifuge Modelling: Two extremes*, 334-345.
- [14] Hall, S. A. (2006). A methodology for 7D warping and deformation monitoring using time-lapse seismic data. *Geophysics*, **71**(4), O21-O31.
- [15] Hall, S. A., Bornert, M., Desrues, J., Pannier, Y., Lenoir, N., Viggiani, G., & Besuelle, P. (2010). Discrete and continuum analysis of localised deformation in sand using X-ray uCT and volumetric digital image correlation. *Geotechnique*, **60**(5), 315–322.
- [16] Silva, M., (2014). Experimental study of ageing and axial cyclic loading effect on shaft friction along driven piles in sand. PhD Thesis University of Grenoble.